Soft Matter

PAPER

View Article Online
View Journal | View Issue

Tri-layer wrinkling as a mechanism for anchoring center initiation in the developing cerebellum

Emma Lejeune,[a] Ali Javili,[a] Johannes Weickenmeier,[b] Ellen Kuhl*[b] and Christian Linder*[a]

Received February 24, 2016

During cerebellar development, anchoring centers form at the base of each fissure and remain fixed in place while the rest of the cerebellum grows outward. Cerebellar foliation has been extensively studied; yet, the mechanisms that control anchoring center initiation and position remain insufficiently understood. Here we show that a tri-layer model can predict surface wrinkling as a potential mechanism to explain anchoring center initiation and position. Motivated by the cerebellar microstructure, we model the developing cerebellum as a tri-layer system with an external molecular layer and an internal granular layer of similar stiffness and a significantly softer intermediate Purkinje cell layer. Including a weak intermediate layer proves key to predicting surface morphogenesis, even at low stiffness contrasts between the top and bottom layers. The proposed tri-layer model provides insight into the hierarchical formation of anchoring centers and establishes an essential missing link between gene expression and evolution of shape.

1 Introduction

The cerebellum, the little brain, is a tightly folded structure located at the bottom of the brain. It plays an important role in motor control and higher order functions including cognition, emotion, and language processing.[1] Unlike the cerebrum, the cerebellum is covered with finely spaced parallel grooves that create a morphologically unique appearance, similar to an accordion,[2] see Fig. 1. When completely unfolded, the cerebellar surface covers an area of 5 cm times 1 m. Although it only accounts for 10% of the total brain volume, the cerebellum contains more neurons than the rest of the brain.[3]

The ridges of the cerebellum are called folia, and their formation during cerebellar development is referred to as foliation.[5] Although cerebellar foliation is intensely studied, the mechanisms that direct the initiation and position of individual folia remain insufficiently understood.[1] In the healthy brain, cerebellar foliation follows a tightly regulated sequence of genetically induced events[2]: At the beginning of foliation, anchoring centers form at the base of each fissure. These centers maintain relatively fixed positions as the cerebellar lobes grow outward.[4] The outer cerebellum undergoes a period of rapid anisotropic growth, with faster growth along the anterior-posterior direction, perpendicular to the folia.[6] Altering specific genes changes the onset and location of the anchoring centers and can modulate surface morphogenesis.[7] Understanding the mechanisms of cerebellar foliation is critical because developmental malformations can affect cerebellar structure and, ultimately, cerebellar function including fine movement, equilibrium, posture, and motor learning.[8]

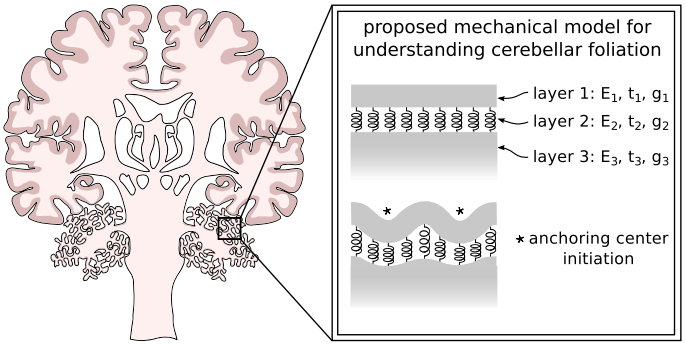

Fig. 1 The cerebellum, the little brain, is a tightly folded structure located at the bottom of the brain. We model cerebellar development using a tri-layer physical model in which anchoring center initiation is a multi-layer wrinkling instability of differential growth between the top and bottom layers.

From a physics perspective, the most appealing explanation for cerebellar foliation is the instability phenomenon of growth-induced surface wrinkling.[9–11] Surface wrinkling in the cerebrum has been modeled using a bi-layer model in which compressive stresses from differential growth induce wrinkling instabilities.[12–15] Bi-layer models are widely used to predict surface morphogenesis and pattern formation in engineering structures,[16] geophysics,[17] soft matter physics,[18] and thin films,[19,20] where

[a] Department of Civil and Environmental Engineering, Stanford University, Stanford, CA 94305, USA. E-mail: linder@stanford.edu
[b] Department of Mechanical Engineering, Stanford University, Stanford, CA 94305, USA. E-mail: ekuhl@stanford.edu

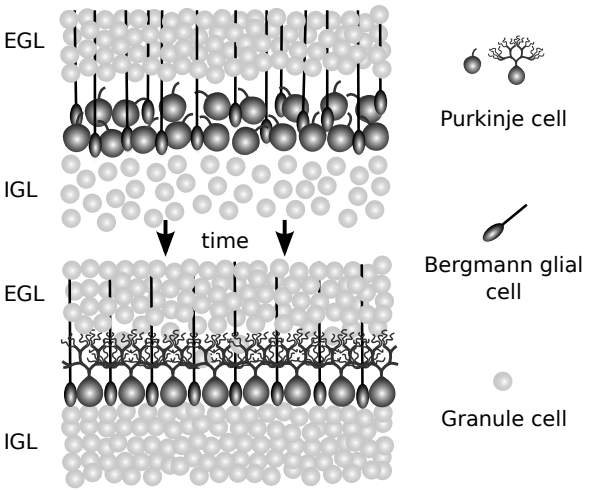

Fig. 2 Evolving layered structure throughout the course of cerebellar development. During development, cells proliferate in the external granular layer (EGL) and migrate to the internal granular layer (IGL).[4] The intermediate Purkinje cell layer changes structure as each cell grows dendrites and the layer transforms from a multi-layer to a mono-layer.[4] At the onset of foliation, the thickness ratio between the EGL and the Purkinje cell layer is much smaller than post-development.

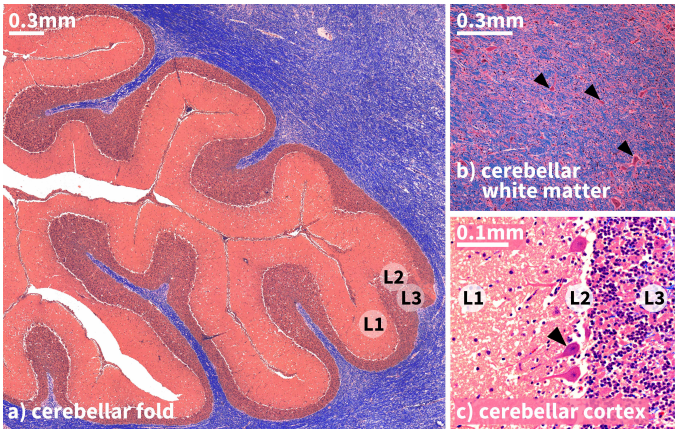

Fig. 3 Sagittal slices of a neonatal mammalian cerebellum stained with luxol fast blue (LFB) and hematoxylin/eosin (H&E) illustrate the three distinct layers of the cerebellum: the external molecular layer (L1), the intermediate Purkinje cell layer (L2), and the internal granular layer (L3). These stains show physical structure post-development, which is significantly different from the structure at the onset of foliation.

the upper layer is orders of magnitude stiffer than the lower layer.[21,22] To measure the stiffness in different regions of the brain, we used nanoindentation[23] and recorded stiffness values of 0.68 ± 0.20 kPa in the outer gray matter layer and 1.41 ± 0.66 kPa in the inner white matter of the cerebrum, a stiffness contrast of less than one half, see Table 1. The bi-layer folding model, however, fails to predict folding for stiffness contrasts smaller than two.[24,25]

Unlike the cerebrum, the cerebellum consists of three distinct surface layers: an external molecular layer, a thin intermediate Purkinje cell layer, and an internal granular layer, shown in Fig. 2. To illustrate these layers in the developed cerebellum, we stained saggital slices of a neonatal mammalian cerebellum with luxol fast blue (LFB) and hematoxylin/eosin (H&E), see Fig. 3. In nanoindentation tests, we found that the cerebellar stiffness of 0.75 ± 0.29 kPa was of same order of magnitude as the cerebral stiffness, see Table 1. These observations motivated our hypothesis that a tri-layer model with a soft intermediate Purkinje cell layer can predict the onset of surface wrinkling and cerebellar foliation, even at low stiffness contrasts between the upper and lower layers.

The rest of the paper is organized as follows. In Section 2 we describe our proposed physical model of the cerebellum. Then, Section 3 discusses the implications of adopting our model to describe the onset of cerebellar foliation. Concluding remarks are given in Section 4.

Table 1 Regional stiffness variation from nanoindentation.

region	cerebrum gray matter	cerebrum white matter	cerebellum gray & white
stiffness [kPa]	0.68 ± 0.20	1.41 ± 0.66	0.75 ± 0.29

2 Model

Here we present our tri-layer model for instability initiation. Previous applications of this tri-layer model involved stiff films adhered to soft substrates, therefore the analytical solution has not been validated in the regime where $E_f \approx E_s$ and the behavior of low-stiffness-contrast tri-layer systems is poorly understood.[30] To address this, we compare the analytical solution to results obtained using the finite element method, described in Section 2.2.

2.1 Analytical model

The essential idea of the tri-layer model is to modify the classical bi-layer film-substrate model[16,17] by reinterpreting the external molecular layer as the film and the combined intermediate layer and internal layer as the substrate.[30] We characterize the tri-layer model through the stiffensses E_f, E_i, and E_s and thicknesses t_f, t_i and t_s of the film, the intermediate layer, and the substrate. We assume that the cerebellum is incompressible with Poisson's ratios of $\nu_f = \nu_i = \nu_s = 0.5$ and that t_s can be treated as infinite. We use the classical Föppl-von Kármán equations[31] to define the stress in the film P as a function of the wavenumber n,

$$P = \frac{E_f t_f^2 n^2}{12} + \frac{K}{t_f n^2} \tag{1}$$

where K is the combined intermediate layer and substrate stiffness,[30]

$$K = \frac{2E_s n}{2nt_i(E_s/E_i - 1) + 4}. \tag{2}$$

The intermediate layer contains Purkinje cells, Bergmann glial cells, and their fibers, see Fig. 4. To account for its pronounced microstructural orientation, we model the intermediate layer as a set of springs.[4,6] With this approach, a tri-layer system with an intermediate layer spring stiffness approaching zero $E_i \to 0$ corresponds to a film, which buckles independently of the substrate

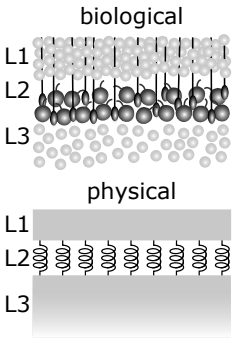

	biological	physical
L1	external molecular layer with rapid growth	film stiffness E_f represents axial and bending strength; fast film growth g_f with $g_\mathrm{f} > g_\mathrm{s}$
L2	Purkinje cell layer with Bergmann glial cells and aligned, unbraced fibers	intermediate stiffness E_i represents smeared spring stiffness in fiber direction with $E_\mathrm{i} < E_\mathrm{f}$
L3	internal granular layer with moderate growth	substrate stiffness E_s represents axial and bending strength with combined E_i and E_s smaller than E_f; moderate substrate growth g_s with $g_\mathrm{s} < g_\mathrm{f}$

Fig. 4 Biological and physical mechanisms of our tri-layer model. Each layer is equipped with its own layer stiffness E, layer thickness t, and growth g. For wrinkling to occur, the external film growth g_f must be greater than the substrate growth g_s and the combined intermediate and substrate stiffnesses E_i and E_s must be less than the film stiffness E_f.

with $K \to 0$, while an intermediate layer stiffness exactly equal to the substrate stiffness $E_\mathrm{i} = E_\mathrm{s}$ recovers the classical bi-layer model where[30]

$$K = \frac{2E_\mathrm{s}}{n}. \tag{3}$$

To determine the critical stress P_cr and the associated critical wave number n_cr, we take the derivative of P with respect to n and set the derivative equal to zero,

$$f(n) = \frac{\mathrm{d}P(n)}{\mathrm{d}n} = \frac{E_\mathrm{f} t_\mathrm{f}^3 n^4}{6} + K'n - 2K \doteq 0 \tag{4}$$

with

$$K' = \frac{8E_\mathrm{s}}{[2nt_\mathrm{i}(E_\mathrm{s}/E_\mathrm{i} - 1) + 4]^2}. \tag{5}$$

We solve the critical condition (4) using an implicit solution scheme and apply Newton's method,

$$f'(n) = \frac{\mathrm{d}^2P(n)}{\mathrm{d}n^2} = \frac{2E_\mathrm{f} t_\mathrm{f}^3 n^3}{3} + K''n - K' \tag{6}$$

with

$$K'' = -\frac{32E_\mathrm{s} t_\mathrm{i}(E_\mathrm{s}/E_\mathrm{i} - 1)}{[2nt_\mathrm{i}(E_\mathrm{s}/E_\mathrm{i} - 1) + 4]^3} \tag{7}$$

to incrementally update the wave number until the critical condition $f(n)$ drops below a defined tolerance. Upon convergence, we calculate the critical stress P_cr using Eqn. (1), and subsequently calculate the critical growth in the film layer and critical wavelength as[30]

$$g_\mathrm{cr} = \frac{P_\mathrm{cr}}{E_\mathrm{f} - P_\mathrm{cr}} \qquad \text{and} \qquad \lambda_\mathrm{cr} = \frac{2\pi}{n_\mathrm{cr}}. \tag{8}$$

The outcome of solving these equations is an understanding of when the wrinkling instability will occur through g_cr, and an understanding of what the instability mode will look like through λ_cr.

2.2 Computational model

A computational model is required to verify the analytical solution in the regime where film and substrate stiffness are approximately equal, $E_\mathrm{f} \approx E_\mathrm{s}$. We develop a computational model by first treating the entire domain as a continuum where behavior is governed by the balance of linear momentum.[32] Then, we discretize the domain and solve for g_cr and λ_cr by performing eigenvalue analysis using the finite element method.[33]

In the continuum setting, we define deformation gradient $\mathbf{F}$ as $\mathbf{F} = \nabla_\mathbf{X}\boldsymbol{\varphi}$ where $\boldsymbol{\varphi}$ is the deformation map, mapping points from the undeformed configuration $\mathbf{X}$ to the deformed configuration $\mathbf{x}$. Then, we multiplicatively decompose the deformation gradient as[34]

$$\mathbf{F} = \mathbf{F}^e\,\mathbf{F}^g \tag{9}$$

where $\mathbf{F}^e$ is the elastic component of deformation and $\mathbf{F}^g$ is the growth component. As with the analytical solution, we only assume growth in the upper most layer. For consistency with experimental observations,[6] we prescribe growth as transversely isotropic[35] in the direction parallel to the anterior-posterior axis of the cerebellum.

In our continuum model, we treat all materials as isotropic and hyperelastic with a Neo-Hookean free energy of the form

$$\psi = \psi(\mathbf{F}^e) = \tfrac{1}{2}\mu[\mathbf{F}^e : \mathbf{F}^e - 3 - 2\ln J^e] + \tfrac{1}{2}\lambda[\tfrac{1}{2}[(J^e)^2 - 1] - \ln J^e] \tag{10}$$

where μ and λ are Lamé material parameters, and J^e is the Jacobian $J^e = \det\mathbf{F}^e$. To capture incompressibility we approximate Poisson's ratio with $\nu = 0.495$. Because unrestrained growth is assumed to be stress free, ψ is expressed as a function of $\mathbf{F}^e$ alone. Additional parameters required to complete our continuum description follow from Eqn. (10).[32,33]

For our computational simulations, we take advantage of the fact that the predominant direction of growth is defined by the anterior-posterior axis of the cerebellum and treat the domain as two-dimensional where the medial-lateral axis is captured by the plane strain condition. Given geometric properties (layer thickness) and material properties (layer modulus) we discretize the domain with quadratic elements and run simulations using an in-house nonlinear finite element code. We are able to compute g_cr and λ_cr by performing eigenvalue analysis on the stiffness matrix of the system. We use the bi-section method to determine the level of growth that causes the stiffness matrix to become singular, g_cr, and examine the associated eigenvector to determine λ_cr.[33]

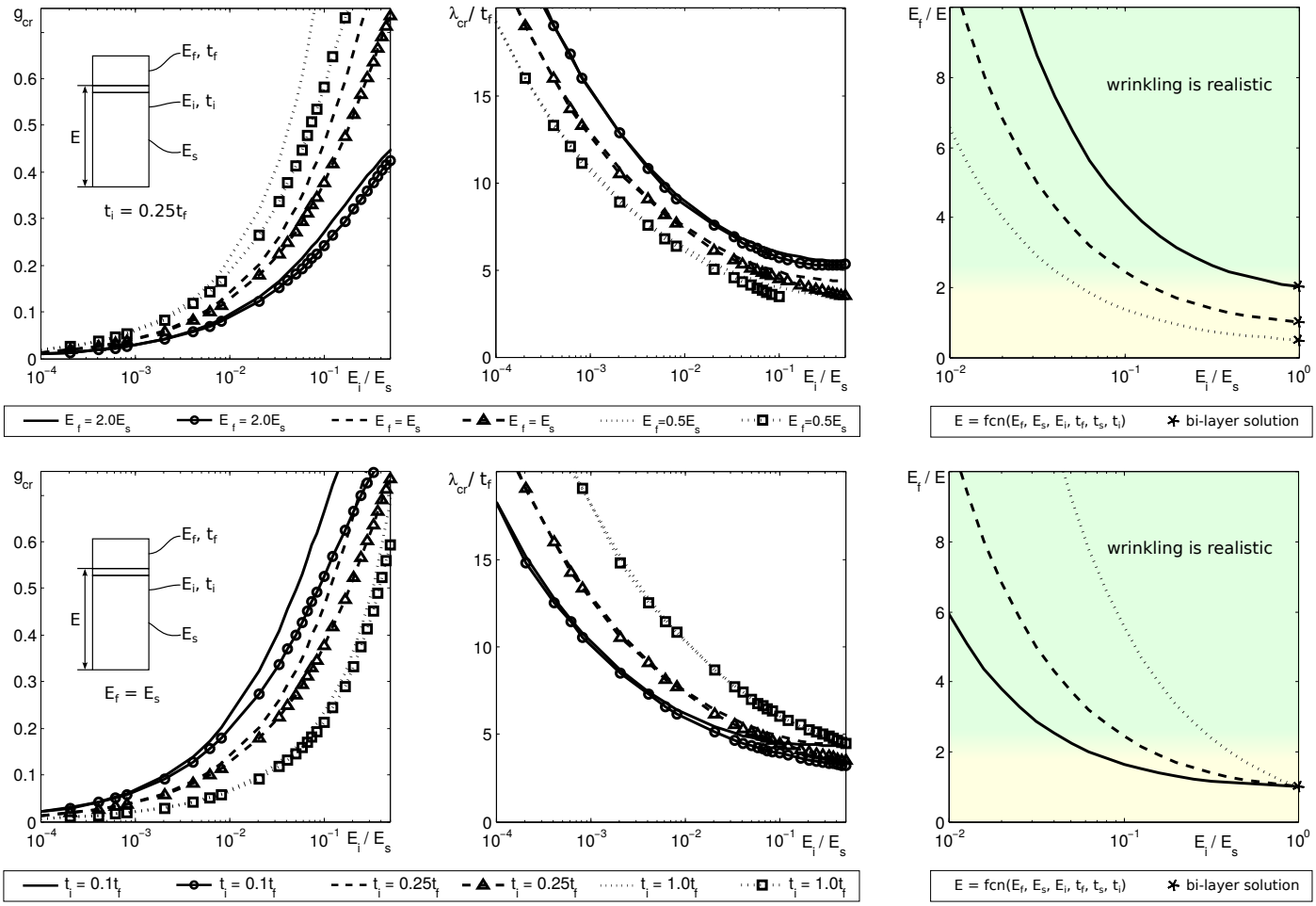

Fig. 5 Critial growth g_{cr}, relative wavelength $\lambda_{\mathrm{cr}}/t_{\mathrm{f}}$, and relative film to combined intermediate layer and substrate stiffness E_{f}/E for varying intermediate layer stiffness E_{i}. Numerical results (symbols) show good agreement with analytical solution, left and center. The upper row of plots demonstrates the sensitivity of g_{cr} and λ_{cr} to the relative film to substrate stiffness $E_{\mathrm{f}}/E_{\mathrm{s}}$ while the lower row demonstrates the sensitivity to layer thickness t_f/t_i. For all cases plotted, t_i is sufficiently low such that our analytical approach remains valid, tri-layer systems with a thicker intermediate layer require additional treatment.[26,27] The plots in the right column show that unlike the classical bi-layer model, the new tri-layer model can predict wrinkling as the likely first mode of instability for low film-to-substrate stiffness contrasts when $E_{\mathrm{f}} \approx E_{\mathrm{s}}$, right. For systems where $E_{\mathrm{f}} \approx E_{\mathrm{i}} \approx E_{\mathrm{s}}$, differential growth combined with surface imperfections will likely cause crease formation prior to wrinkling.[28,29]

Fig. 5 shows representative numerical results where each point plotted (marked with symbols) represents one simulation run. The plots in Fig. 5, left and center columns, indicate that the analytical and numerical solutions are in excellent agreement. In future work, the computational model will be required because the analytical solution uses the small strain assumption, assumes a flat domain, and ignores boundary effects. Furthermore, to quantitatively describe and predict folia formation beyond the onset of the instability, we would have to use an entirely numerical approach.

3 Results and discussion

Fig. 5, right, demonstrates that unlike the bi-layer model, the tri-layer model can realistically predict wrinkling at low stiffness contrasts when $E_{\mathrm{f}} \approx E_{\mathrm{s}}$. Fig. 6 illustrates how instability initiation can serve as a mechanism to explain anchoring center initiation. Consistent with experimental observations where multiple anchoring centers form in unison,[4] the coordinated appearance of anchoring centers can be attributed to simultaneously reaching the critical growth value g_{cr}. The associated critical wavelength λ_{cr} dictates the number of anchoring centers. Anchoring centers form at the troughs of the emerging instability pattern. Cells located in the troughs experience compression and an altered physical environment, which could potentially induce further changes in cell behavior and gene expression.[36,37]

Interpreting surface instabilities as the mechanism by which anchoring centers form opens a new path for correlating gene expression to cerebellar foliation. For example, genes that are related to altering the timing of anchoring center formation are immediately connected to changes in the number of anchoring centers and to the cerebellar morphology at the end of development.[4] Studies suggest that this final morphology is highly sensitive to the granular cell proliferation rate,[38] the thickness of the external granular layer, and the number of primary lobules.[39] Our physics-based model for anchoring center initiation makes the connection between timing, through g_{cr}, and shape, through

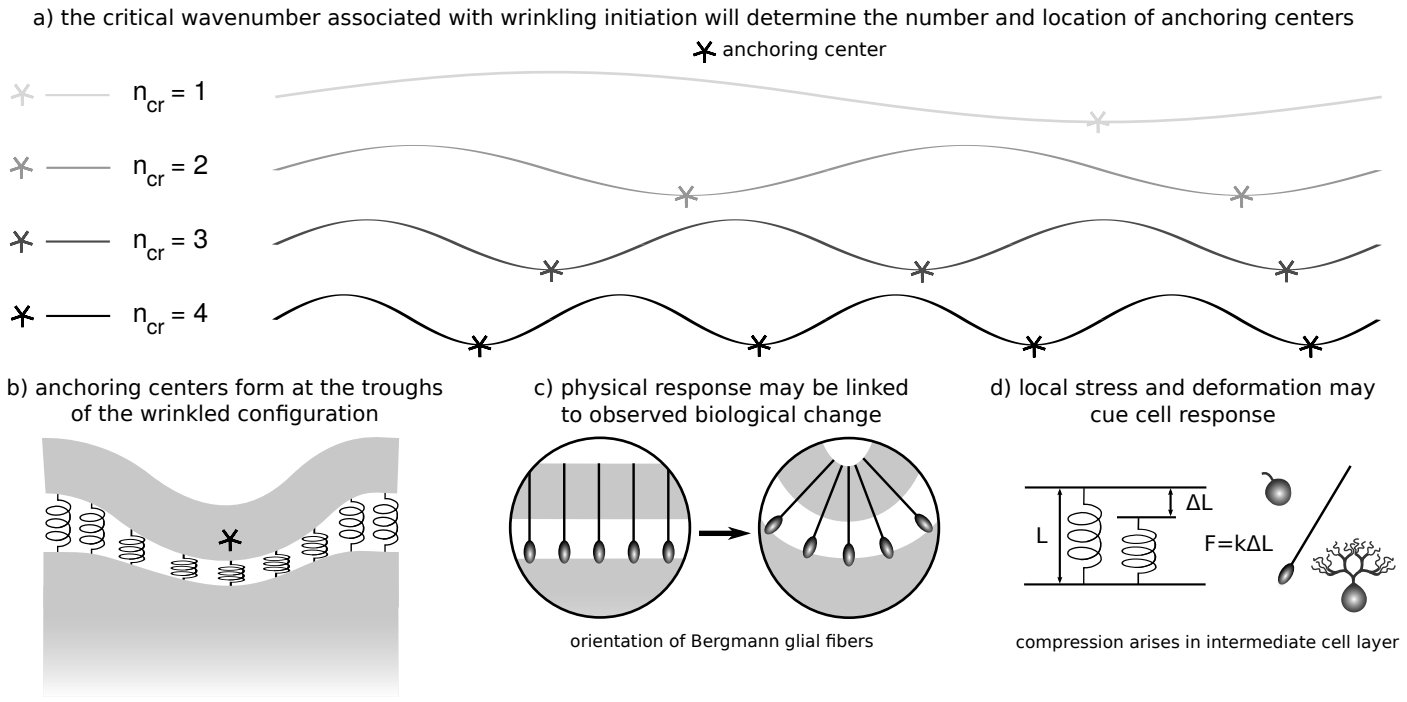

Fig. 6 (a) The wave number $n_{\mathrm{cr}} = 2\pi/\lambda_{\mathrm{cr}}$, and with it the number of anchoring centers, is sensitive to the layer stiffness as predicted in Fig. 5, center. The folding patterns are the eigenvectors of the wrinkling instability mode. (b) Anchoring centers form at the troughs of the sine waves. (c) Bergmann glial fibers, here represented through springs, fan out from the base of the anchoring center.[4] (d) Cells at the anchoring centers in the intermediate layer experience compression, which may influence cell behavior and induce changes in gene expression that further drive the foliation process.

λ_{cr}, straightforward. From Eqs. (1) and (2) and Fig. 7 it is clear that E_{f}, E_{i}, E_{s}, t_{f}, and t_{i} influence timing g_{cr} and shape λ_{cr}. In addition, the ratio between film and substrate growth, g_{f} and g_{s}, influences instability initiation.[32] The physical model allows us to formalize these correlations between altered gene expression and evolution of shape.

With regard to the connection between tri-layer wrinkling and the hierarchical anchoring center formation that defines lobules and sublobules, there are two significant additional considerations: First, after anchoring centers form, when the external and intermediate layers buckle out of plane, further outward growth can occur without building up substantial compressive stresses.[9] However, recent studies have shown that cell dispersal at the anchoring centers is blocked,[6] which suggests that anchoring centers act as a growth-constraining boundary conditions that shape the individual lobes, lobules, and sublobules. Second, as the cerebellum develops, the geometric and material properties of each layer change, which will locally alter the critical growth g_{cr} and critical wave length λ_{cr}. Limited cell dispersal across the anchoring centers may produce genetically distinct folia with distinct critical growth g_{cr} and wavelength λ_{cr}.[6] This suggests that g_{cr} and λ_{cr} display significant regional and temporal variations across the developing cerebellum.

Moving forward, the extension of our model for anchoring center initiation to curved geometries, which has already been done for bi-layer systems,[40,41] may provide further insight by more closely resembling the surface of the cerebellum at the onset of foliation. On a similar note, a third layer between the film and the substrate may influence the initiation of other types of geometric instability such as creases.[42–44] Finally, the relationship and coupling between biologically driven processes and mechanically driven processes after anchoring center initiation in the post-buckling regime merits further examination.

4 Conclusion

In this paper, we modeled the initiation of the foliation process during cerebellar development using a physics-based tri-layer model. Unlike classical bi-layer models, this new tri-layer model can predict surface wrinkling, even if the stiffnesses of the inner and outer layer are nearly identical. We demonstrated that tri-layer wrinkling is a realistic mechanism for controlling anchoring center initiation and position. We correlated the parameters that control morphogenesis and pattern formation to cellular events and to changes in gene expression. Understanding the mechanisms of cerebellar foliation is critical to interpret developmental malformations associated with movement, equilibrium, posture, and motor learning. This letter provides a new physical perspective to the phenomenon of cerebellar foliation, which has predominantly been studied through a biological lens.

Acknowledgments

Financial support for this research was provided by the National Science Foundation through CAREER Award CMMI-1553638, the National Science Foundation Graduate Research Fellowship under Grant No. DGE-114747, and the Stanford BioX IIP Grant "Understanding Gyrification Dynamics in the Human Brain".

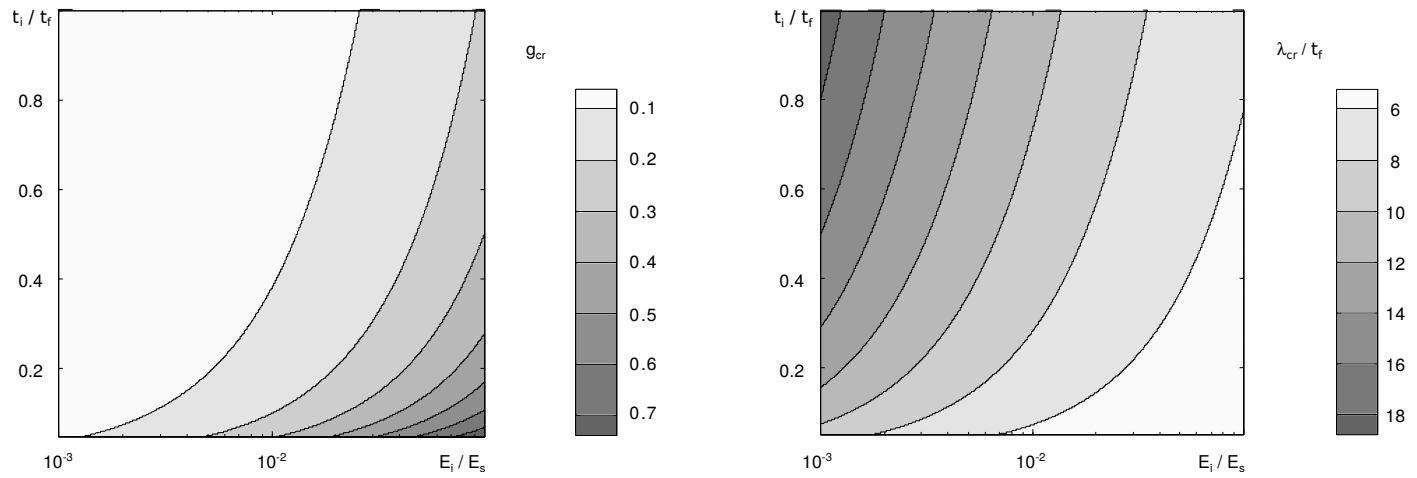

Fig. 7 Timing of anchoring center initiation through $g_{\rm cr}$, left, and position of anchoring centers through $\lambda_{\rm cr}$, right, are altered by changes in material properties $E_{\rm i}/E_{\rm s}$ and geometric properties $t_{\rm i}/t_{\rm f}$. Increasing $K_{\rm i} = E_{\rm i}/t_{\rm i}$ increases $g_{\rm cr}$, left, and decreases $\lambda_{\rm cr}$, right. Understanding that geometric instability may be the cause of anchoring center formation establishes a link between parameters which predict $g_{\rm cr}$ and $\lambda_{\rm cr}$ and the foliation pattern. Both plots correspond to the case where $E_{\rm f} = E_{\rm s}$.

References

1 K. Leto, M. Arancillo, E. B. E. Becker, A. Buffo, C. Chiang, B. Ding, W. B. Dobyns, I. Dusart, P. Haldipur, M. E. Hatten, M. Hoshino, A. L. Joyner, M. Kano, D. L. Kilpatrick, N. Koibuchi, S. Marino, S. Martinez, K. J. Millen, T. O. Millner, T. Miyata, E. Parmigiani, K. Schilling, G. Sekerková, R. V. Sillitoe, C. Sotelo, N. Uesaka, A. Wefers, R. J. T. Wingate and R. Hawkes, *The Cerebellum*, 2015, 1–40.

2 J. D. Corrales, *Development*, 2004, **131**, 5581–5590.

3 R. R. Llinas, K. D. Walton and E. J. Lang, in *The Synaptic Organization of the Brain*, ed. G. M. Shepherd, Oxford University Press, New York, 2004, pp. 339–394.

4 A. Sudarov and A. L. Joyner, *Neural Development*, 2007, **2**, 26.

5 J. D. Corrales, S. Blaess, E. M. Mahoney and A. L. Joyner, *Development*, 2006, **133**, 1811–1821.

6 E. Legue, E. Riedel and A. L. Joyner, *Development*, 2015, **142**, 1661–1671.

7 S. Martinez, A. Andreu, N. Mecklenburg and D. Echevarria, *Frontiers in Neuroanatomy*, 2013, **7**, 18.

8 S. Patel and A. J. Barkovich, *American Journal of Neuroradiology*, 2002, **23**, 1074–1087.

9 A. Goriely and M. BenAmar, *Physical Review Letters*, 2005, **94**, 198103.

10 M. BenAmar and A. Goriely, *Journal of the Mechanics and Physics of Solids*, 2006, **53**, 2284–2319.

11 T. Tallinen, J. S. Biggins and L. Mahadevan, *Physical Review Letters*, 2013, **110**, 024302.

12 D. P. Richman, R. M. Stewart, J. W. Hutchinson and V. S. Caviness, *Science*, 1975, **189**, 18–21.

13 A. Goriely, M. G. D. Geers, G. A. Holzapfel, J. Jayamohan, A. Jérusalem, S. Sivaloganathan, W. Squier, J. A. W. van Dommelen, S. Waters and E. Kuhl, *Biomechanics and Modeling in Mechanobiology*, 2015, 931–965.

14 T. Tallinen, J. Y. Chung, F. Rousseau, N. Girard, J. Lefevre and L. Mahadevan, *Nature Physics*, 2016, in press.

15 E. Kuhl, *Nature Physics*, 2016, in press.

16 H. G. Allen, *Analysis and Design of Structural Sandwich Panels*, Pergamon Press, Oxford, 1969.

17 M. A. Biot, *Journal of Applied Mathematics and Mechanics*, 1937, **22**, 984–988.

18 B. Li, Y.-P. Cao, X.-Q. Feng and H. Gao, *Soft Matter*, 2012, **8**, 5728.

19 J. W. Hutchinson, *Philosphical Transactions of the Royal Society A*, 2014, **371**, 20120422.

20 H. Mei, R. Huang, J. Y. Chung, C. M. Stafford and H. H. Yu, *Applied Physics Letters*, 2007, **90**, 151902.

21 P. Ciarletta, V. Balbi and E. Kuhl, *Physical Review Letters*, 2014, **113**, 248101.

22 L. Jin, A. Takei and J. W. Hutchinson, *Journal of the Mechanics and Physics of Solics*, 2015, **81**, 22–40.

23 S. Budday, R. Nay, R. de Rooij, P. Steinmann, T. Wyrobek, T. C. Ovaert and E. Kuhl, *Journal of the Mechanical Behavior of Biomedical Materials*, 2015, **46**, 318–30.

24 E. Hohlfeld and L. Mahadevan, *Physical Review Letters*, 2011, **106**, 105702.

25 S. Budday, E. Kuhl and J. W. Hutchinson, *Philosophical Magazine*, 2015, **95**, 3208–3224.

26 E. Lejeune, A. Javili and C. Linder, *Extreme Mechanics Letters*, 2016, in press.

27 Z. Wu, J. Meng, Y. Liu, H. Li and R. Huang, *Journal of Applied Mechanics*, 2014, **81**, 081003.

28 Y. Cao and J. W. Hutchinson, *Proc. R. Soc. A*, 2012, **468**, 94–115.

29 F. Weiss, C. S., Y. Hu, M. Kang and R. Huang, *Journal of Applied Physics*, 2013, **114**, 073507.

30 E. Lejeune, A. Javili and C. Linder, *Soft Matter*, 2016, **12**, 806–816.

31 J. Dervaux and M. BenAmar, *Physical Review Letters*, 2008,

101, 068101.
32 S. Budday, P. Steinmann and E. Kuhl, *Journal of the Mechanics and Physics of Solids*, 2014, **72**, 75–92.
33 A. Javili, B. Dortdivanlioglu, E. Kuhl and C. Linder, *Computational Mechanics*, 2015, **56**, 405–420.
34 E. Rodriguez, A. Hoger and A. McCulloch, *Journal of Biomechanics*, 1994, **27**, 455–467.
35 S. Göktepe, O. J. Abilez and E. Kuhl, *Journal of the Mechanics and Physics of Solics*, 2010, **58**, 1661–1680.
36 L. Jiang, C. Yang, L. Zhao and Q. Zheng, *Soft Matter*, 2014, **10**, 4603.
37 X. Zeng and S. Li, *Soft Matter*, 2012, **8**, 5765.
38 V. Mares and Z. Lodin, *Brain Research*, 1970, **23**, 343–352.
39 M. L. Doughty, N. Delhaye-Bouchaud and J. Mariani, *The Journal of Comparative Neurology*, 1998, **399**, 306–320.
40 Y. P. Cao, B. Li and X. Q. Feng, *Soft Matter*, 2012, **8**, 556–562.
41 X. Chen and J. Yin, *Soft Matter*, 2010, **6**, 5667–5680.
42 S. Cai, D. Chen, Z. Suo and R. C. Hayward, *Soft Matter*, 2012, **8**, 1301.
43 T. Tallinen, J. Y. Chung, J. S. Biggins and L. Mahadevan, *PNAS*, 2014, **111**, 12667.
44 Z. Wu, N. Bouklas and R. Huang, *International Journal of Solids and Structures*, 2012, **50**, 578–587.